Unraveling the transcriptome profile of pulsed electromagnetic field stimulation in bone regeneration using a bioreactor-based investigation platform

(Article begins on next page)

11 October 2024
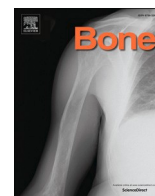
Full Length Article

Unraveling the transcriptome profile of pulsed electromagnetic field stimulation in bone regeneration using a bioreactor-based investigation platform

Farah Daou [a], Beatrice Masante [b,c], Stefano Gabetti [b,c], Federico Mochi [d], Giovanni Putame [b,c], Eleonora Zenobi [d,e], Elisa Scatena [d,e], Federica Dell'Atti [a], Francesco Favero [a], Massimiliano Leigheb [a,f], Costantino Del Gaudio [g], Cristina Bignardi [b,c], Diana Massai [b,c], Andrea Cochis [a], Lia Rimondini [a,*]

[a] Dept. of Health Sciences, Center for Translational Research on Autoimmune and Allergic Diseases (CAAD), Università del Piemonte Orientale (UPO), Novara, Italy
[b] Dept. of Mechanical and Aerospace Engineering, PolitoBIOMed Lab, Politecnico di Torino, Turin, Italy
[c] Interuniversity Center for the Promotion of the 3Rs Principles in Teaching and Research, Pisa, Italy
[d] Hypatia Research Consortium, Rome, Italy
[e] E. Amaldi Foundation, Rome, Italy
[f] Department of Orthopaedics and Traumatology, "Maggiore della Carità" Hospital, Novara, Italy
[g] Italian Space Agency, Rome, Italy

ARTICLE INFO

ABSTRACT

Introduction: Human mesenchymal stem cells (hMSCs) sense and respond to biomechanical and biophysical stimuli, yet the involved signaling pathways are not fully identified. The clinical application of biophysical stimulation including pulsed electromagnetic field (PEMF) has gained momentum in musculoskeletal disorders and bone tissue engineering.
Methodology: We herein aim to explore the role of PEMF stimulation in bone regeneration by developing trabecular bone-like tissues, and then, culturing them under bone-like mechanical stimulation in an automated perfusion bioreactor combined with a custom-made PEMF stimulator. After selecting the optimal cell seeding and culture conditions for inspecting the effects of PEMF on hMSCs, transcriptomic studies were performed on cells cultured under direct perfusion with and without PEMF stimulation.
Results: We were able to identify a set of signaling pathways and upstream regulators associated with PEMF stimulation and to distinguish those linked to bone regeneration. Our findings suggest that PEMF induces the immune potential of hMSCs by activating and inhibiting various immune-related pathways, such as macrophage classical activation and MSP-RON signaling in macrophages, respectively, while promoting angiogenesis and osteogenesis, which mimics the dynamic interplay of biological processes during bone healing.
Conclusions: Overall, the adopted bioreactor-based investigation platform can be used to investigate the impact of PEMF stimulation on bone regeneration.

1. Introduction

The endogenous electromagnetic field (EMF) plays decisive roles at the cellular and molecular levels, including those of the musculoskeletal system that are often in the form of pulsed EMF (PEMF) and are known to induce osteogenesis. From this perspective, exogenous PEMF stimulation has been applied to stimulate the natural streaming potentials in bone and to promote bone regeneration and repair [1]. This provoked PEMF, and biophysical stimulation in general, as the "new pharmacology" for being a non-invasive therapy not only with osteogenic properties, but also with chondrogenic and anti-inflammatory ones [2]. In response to the clinical translation of bone growth stimulators based on PEMF and the accumulation of data on their safety and efficacy, the Food and Drug Administration (FDA) reclassified them from Class III to

Class II devices in 2020 [3]. The most established clinical application of PEMF is the treatment of musculoskeletal disorders mainly delayed union or nonunion fractures, osteoarthritis, osteoporosis, osteonecrosis, and tendon disorders, [4] in addition to musculoskeletal chronic pain including low back pain [5]. In tandem with the previously mentioned clinical applications, researchers have been exploring the efficacy and safety of PEMF stimulation in various disorders in an attempt to broaden its indications, and examples include postoperative pain and edema after plastic surgery [6], treatment-resistant depression [7], and oncology [8].

Subsequently, scientists combined PEMF stimulation with biomaterials for bone tissue engineering (BTE) to produce functional bone grafts and to ameliorate the clinical outcomes of BTE applications [9]. Despite the accumulation of supporting evidence, the diversity of the EMF stimuli relating to frequencies, intensities, waveforms, and durations of exposure, as well as the heterogeneity of the biomaterials, warrant a more in-depth exploration [10].

Akin to the progress that has been made in expanding the preclinical and clinical application of PEMF, significant progress has been made in uncovering the various signaling pathways underlying its physiological effects. Although both in vitro and in vivo studies revealed the cellular and molecular mechanisms associated with the PEMF stimulation of osteogenesis, chondrogenesis, and anti-inflammation, a great deal still needs to be done to have a comprehensive overview of the signaling pathways through which PEMF exert its physiological effects, and until then, the basis for its clinical use remains not solid or wholesome [11–13]. Moreover, PEMF stimulation must overcome a significant hurdle to wide clinical application, and that is the absence of standardized clinical practice guidelines, since the optimal clinical PEMF stimulation parameters for each disorder are still not set [14,15]. An additional factor that should not be overlooked is the possible health risks linked to the exposure to PEMF in routine clinical settings for both healthcare providers and patients [16,17].

With the purpose of tackling the knowledge gap in PEMF research, the objective of our study was to explore the effects of PEMF stimulation on stem cell behavior and osteogenic commitment. To achieve this, we utilized an in vitro biomimetic investigation platform, recently proposed by the Authors [18], based on an automated perfusion bioreactor that provides bone-tissue-like mechanical stimulation (i.e., fluid flow-induced shear stress) and can be equipped with a custom-made PEMF stimulator. First, we developed trabecular bone-like tissues, consisting of 3D-printed biomimetic polylactic acid (PLA) scaffolds and human bone marrow-derived mesenchymal stem cells (BM-MSCs) seeded on the scaffolds. We conducted experiments to evaluate the efficacy of different cell seeding methods and culture media. Afterward, we employed the most adequate conditions to investigate the impact of PEMF stimulation on BM-MSCs cultured under bone-like mechanical stimulation provided by the automated perfusion bioreactor via transcriptomic studies. The latter was performed since understanding the signaling pathways involved in the effects of PEMF stimulation is crucial for identifying the underlying cellular and molecular mechanisms related to bone regeneration and repair. We hypothesized that PEMF stimulation could induce stem cell osteogenic commitment via unconventional signaling pathways, and that the in vitro investigation platform can allow us to acquire knowledge that would aid in getting deeper insights into the optimal clinical applications of PEMF stimulation for bone regeneration and repair, which in turn can help in reducing the number of animals used in bone biology research. Our results showed that PEMF exposure increased the osteogenic commitment of BM-MSCs, and the transcriptomic studies revealed a complex interplay of various signaling pathways involved in the immune potential, osteogenic potential, and angiogenic potential of BM-MSCs following exposure to PEMF.

2. Methodology

2.1. 3D printing and characterization of the biomimetic polylactic acid (PLA) scaffolds

The design and fabrication of the 3D-printed, biomimetic PLA scaffolds have been carried out according to a previously reported procedure [19]. Briefly, a random 3D distribution of spheres, as virtual porogens with a diameter of 600 μm, was created by means of a custom-made script to be subtracted from a cylindrical volume (10 mm diameter, 5 mm height) to prepare the scaffold computer-aided design (CAD) models. The resulting files were imported to ideaMaker (Raise3D Inc., Irvine, CA, USA) and sliced in the Z direction at 0.25 mm. Scaffolds were then fabricated by processing a PLA filament (FormFutura BV, The Netherlands) using a Raise 3D N2 printer (Raise 3D Inc., Irvine, CA, USA), setting the nozzle temperature at 205 °C and the build plate temperature at 60 °C. The scaffolds were previously characterized and tested for bioactivity [20]. The resulting scaffolds have a mean permeability value of 2.36×10^{-10} m^2 [21].

2.2. Parallelized, automated perfusion bioreactor equipped with PEMF stimulator

An automated perfusion bioreactor equipped with a custom-made PEMF stimulator, previously developed and described [18], was here parallelized. Briefly, the parallelized, automated perfusion bioreactor consists of three independent 3D-printed culture chambers (CCs) connected to three independent closed-loop hydraulic circuits controlled by a custom control unit, designed for housing and culturing the 3D bone-like tissues under direct perfusion (Fig. 1). Direct perfusion guarantees continuous medium flow through the cultured constructs, ensuring efficient mass transport and exposing the constructs to fluid flow-induced shear stress, which is known to promote proliferation and differentiation of osteoblasts and to favor bone mineralization [22,23].

Each CC (Dental SG Resin, Formlabs, United States) is composed of two screwable parts that allow housing constructs of different sizes, which are in turn press-fit in a tailored polydimethylsiloxane (PDMS) holder (SYLGARD 184, Dow Corning, United States). Each closed loop hydraulic circuit is composed of oxygen-permeable tubing (Darwin Microfluidics, France) and a culture medium reservoir, and is connected to a multichannel peristaltic pump (G100–1 J, Longer Precision Pump, China) suitable to be incubated at 37 °C. The pump is controlled by a custom control unit, equipped with a microcontroller board (Arduino Micro, Arduino, Italy), that allows setting the pump's parameters and guarantees the same perfusion conditions in each CC. Finally, the custom-made PEMF stimulator (IGEA Clinical Biophysics, Italy) consists of a generator and two solenoids among which the bioreactor CCs can be placed (magnetic field intensity = 1.5 mT, frequency = 75 Hz).

2.3. Trabecular bone-like tissue preparation and evaluation

2.3.1. Cell culture conditions

Human telomerase reverse transcriptase (hTERT)-immortalized BM-MSCs of clonal line Y201, which was generated by James et al. [24], were cultivated in basal medium (BM) that is low-glucose Dulbecco's modified Eagle's medium (DMEM, Gibco, Thermo Fisher Scientific, Inc.) supplemented with 15 % fetal bovine serum (FBS, Gibco Thermo Fisher Scientific, Inc.) and 1 % antibiotics (penicillin/streptomycin, Gibco Thermo Fisher Scientific, Inc.) incubated in a humidified atmosphere with 5 % CO_2 at 37 °C. The cells were passaged once they reached 80–90 % confluency by enzymatic digestion using trypsin/ethylenediamine tetraacetic acid (trypsin/EDTA, Gibco Thermo Fisher Scientific, Inc.) prior to each assay.

2.3.2. Cell seeding and culturing under two conditions

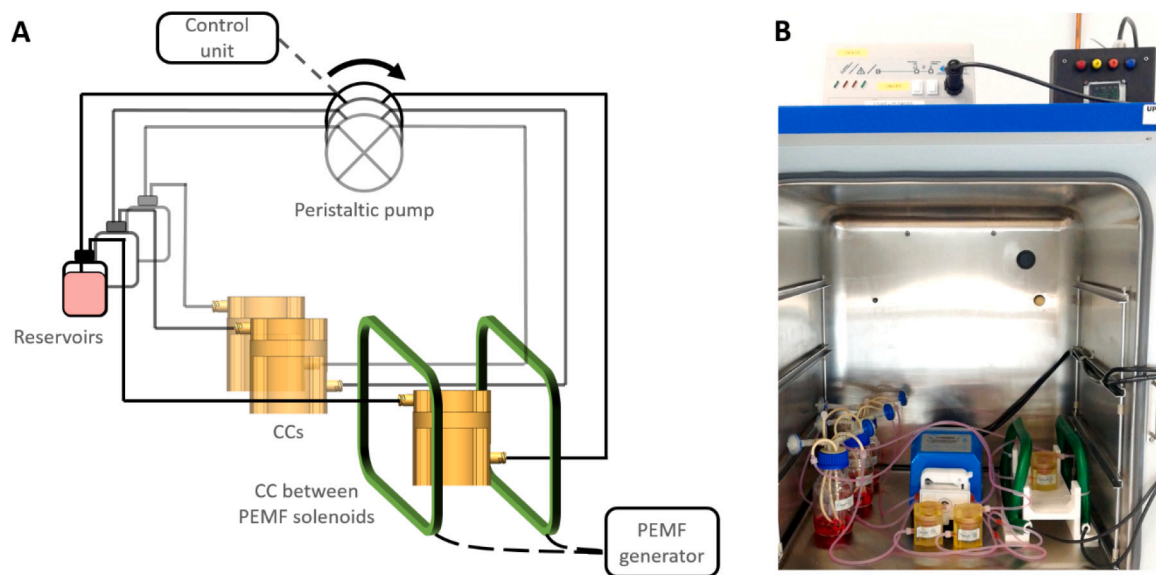Cells were directly seeded on the top of the PLA scaffolds inserted in

Fig. 1. The bioreactor-based investigation platform. **(A)** Schematic representation of the parallelized, automated perfusion bioreactor and the custom-made pulsed electromagnetic field (PEMF) stimulator set-up, with three independent culture chambers and hydraulic circuits; **(B)** Parallelized, automated perfusion bioreactor and PEMF stimulator set-up within the incubator.

the PDMS holders of the automated bioreactor placed in a 6-well cell culture plate either by suspension seeding or by using cell-releasing hydrogels at a defined density of 3×10^6 cells and a defined volume of 200 μL. For suspension seeding, cells were resuspended in 200 μL of BM; for cell-releasing 2 % alginate, 4 % (40 mg/mL) alginate solution was prepared using alginic acid sodium salt from brown algae (Medium viscosity, Merck, Italy), and then mixed in a 1:1 ratio with the cell suspension; and for cell-releasing 0.5 % collagen, cells were resuspended in 200 μL of 5 mg/mL PureCol EZ Gel solution (Merck, Italy). Samples were incubated for 4 h to allow cell infiltration and adhesion. Then, samples seeded by suspension seeding and cell-releasing 0.5 % collagen were covered by BM and incubated overnight; whereas samples seeded by cell-releasing 2 % alginate were incubated overnight in 150 μL of 0.2 M calcium chloride ($CaCl_2$) solution, and then washed once with phosphate-buffered saline (PBS, $1\times$) to remove the $CaCl_2$ solution. After the overnight incubation, the samples were cultured in two different culture conditions for 21 days: static culture, in which the samples were kept in the cell culture plate, and BM was changed every 3–4 days; and direct perfusion, in which samples were placed in the automated perfusion bioreactor under unidirectional, direct perfusion at 0.3 mL/min with 50 mL of BM pumped from the reservoir, and the medium was changed every 7 days. Samples were evaluated in triplicates ($n = 3$).

2.3.3. Cell viability assay

On day 21 of culturing, the viability of BM-MSCs seeded on the biomimetic PLA scaffolds using the three different cell seeding methods and cultured under the two different culture conditions was evaluated via the live/dead cell assay (LIVE/DEAD™ Viability/Cytotoxicity Kit for mammalian cells, Invitrogen Life Technologies). Briefly, the samples were removed from the CCs of the bioreactor, placed in a 24-well cell culture plate, washed with PBS ($1\times$), and then incubated in a BM containing 2 μM calcein-AM and 2 μM ethidium homodimer-1 (EthD-1). After 15 min of incubation at 37 °C and 5 % CO_2 atmosphere, cells were imaged using a fluorescence microscope (THUNDER Imager 3D Cell Culture, Leica Microsystems) to visualize the green calcein AM that stains live cells and the red EthD-1 that stains dead cells.

2.3.4. Cell infiltration and distribution assessment

On day 21 of culturing, the infiltration and distribution of BM-MSCs were examined using a scanning electron microscope (SEM) (JSM-

IT500, JEOL, Italy). For SEM analysis, the samples were removed from the CCs of the bioreactor, placed in a 24-well cell culture plate, and gently washed with PBS ($1\times$). Then, cells were fixed with 2.5 % glutaraldehyde at 4 °C overnight, and after cell fixation, the 2.5 % glutaraldehyde was dispensed, and samples were washed with PBS ($1\times$), dehydrated in graded alcohol of 30 %, 50 %, 70 %, 90 %, and 100 % (twice) for 30 min each, covered by hexamethydisilazane (HMDS) for 30 min, and then air-dried in a chemical fume hood. Finally, samples were coated with gold using a sputter coating machine (DII-29030SCTR Smart Coater, JEOL, Italy).

2.4. Trabecular bone-like tissue stimulation using PEMF

Following the selection of the optimal cell seeding method, which is cell-releasing 0.5 % collagen, the bioreactor-based investigation platform was used to perform preliminary studies on PEMF stimulation for bone healing.

2.4.1. Trabecular bone-like tissue culturing under six conditions

Cells were directly seeded on the top of the PLA scaffolds inserted in the PDMS holders of the bioreactor placed in a 6-well cell culture plate by using cell-releasing 0.5 % collagen at a defined density of 3×10^6 cells and a defined volume of 200 μL, as described in Section 2.3.2. The samples were cultured for 21 days either in BM or osteogenic medium (OM) (low-glucose DMEM supplemented with 10 % FBS, 1 % antibiotics, 20 mM β-glycerophosphate, 50 μM ascorbic acid-2-phosphate, and 10^{-7} M dexamethasone). Samples in BM and OM were cultured in three different culture conditions: static culture, in which the samples were kept in the cell culture plate, and BM or OM was changed every 3–4 days; direct perfusion, in which samples were placed in the automated bioreactor under unidirectional, direct perfusion at 0.3 mL/min with 50 mL of BM or OM pumped from the reservoir, and the media were changed every 7 days; and direct perfusion with PEMF stimulation, in which samples were placed in the automated bioreactor under unidirectional, direct perfusion at 0.3 mL/min with 50 mL of BM or OM pumped from the reservoir, and media were changed every 7 days, accompanied by PEMF stimulation (1.5 mT, 75 Hz) for 4 h per day (corresponding to a cumulative dose of around 75 h over a period of 21 days). Samples were evaluated in triplicates ($n = 3$).

2.4.2. Gene expression analyses

To evaluate osteogenesis, reverse transcription-quantitative PCR (RT-qPCR) was performed. First, the total RNA was extracted using TRIzol™ Reagent (Invitrogen Life Technologies) according to the manufacturer's instructions, except for allowing cell lysing for 10 min instead of 5 min, and the RNA yield and quality were assessed using a NanoDrop spectrophotometer (NanoDrop One, Thermo Fisher Scientific Inc.). Second, 1 μg of total RNA was treated with DNase I to remove genomic DNA contamination and was reverse transcribed using the iScript™ gDNA Clear cDNA Synthesis Kit (Bio-Rad Laboratories) and a thermal cycler (Mastercycler X50s, Eppendorf). Third, the genes of interest and the reference gene were analyzed via qPCR which was performed on 1 ng/μL of cDNA using a master mix of SsoAdvanced™ Universal SYBR® Green Supermix (Bio-Rad Laboratories) and primers at a concentration of 2.5 μM, and the reactions were performed and monitored using a thermal cycler (CFX96™ Real-Time System, Bio-Rad Laboratories) according to the standard protocol. The cycle threshold for each gene of interest was normalized against the reference gene that is glyceraldehyde 3-phosphate dehydrogenase (GAPDH), and relative gene expression levels were determined using the Livak's method ($2^{-\Delta\Delta Cq}$) [25,26] compared with the corresponding control group. This part of the gene expression analyses was aimed at helping in the selection of the culture medium, thus, we investigated the effects of PEMF stimulation in two different culture media: BM and OM. For this purpose, collagen type I alpha 1 chain (COL1A1), osteopontin (OPN), osteocalcin (OCN) and runt-related transcription factor 2 (RUNX2) were used as markers of osteogenesis; whereas, collagen type II alpha 1 chain (COL2A1) was used as a marker of chondrogenesis. The primer pairs of the analyzed genes are listed in Table S1.

Gene expression analyses were also performed following the transcriptomic studies to validate the raw expression signals of 11 genes that are commonly investigated in the literature, and the differential expression of 3 genes that served as a validation of the RNA-Seq, detailed in Section 2.5. The raw expression signals of the following genes were evaluated: the adenosine receptors A_{2A} adenosine receptor (A_{2A}AR), A_{2B} adenosine receptor (A_{2B}AR), and A3 adenosine receptor (A3AR); the member of the Wnt/β-catenin signaling pathway that is Wnt family member 1 (WNT1); the epigenetic factor that is microRNA 26a-1 (miR26A1); the markers of osteogenesis that are OCN and RUNX2; and finally, the markers of angiogenesis that are intercellular adhesion molecule 1 (ICAM1) and kinase insert domain receptor (KDR). The differential expression of the following genes was evaluated: the marker of osteogenesis, OPN; the marker of chondrogenesis, SRY-Box transcription factor 9 (SOX9); and the marker of angiogenesis, platelet and endothelial cell adhesion molecule 1 (PECAM1). The primer pairs of the analyzed genes are listed in Table S1.

2.5. Transcriptomic studies: RNA-sequencing (RNA-Seq)

Based on the results obtained from the first part of the gene expression analyses, the trabecular bone-like tissues cultured for 21 days in BM were selected for transcriptomic studies, since the biochemical signals provided by the OM obscured the detection of the cellular changes caused by PEMF stimulation. Thus, for this part of the experiment, samples were prepared and cultivated in BM for 21 days under three culture conditions, as detailed in Section 2.4.1, and were evaluated in duplicates ($n = 2$). The samples were labelled as follows: "S" represents static culture, "D" represents direct, unidirectional perfusion, and "P" represents direct, unidirectional perfusion with PEMF stimulation.

2.5.1. RNA purification and quality assessment

Total RNA was isolated using TRIzol™ Reagent (Invitrogen Life Technologies) as described in Section 2.4.2, and then purified with the Qiagen RNeasy Mini Kit (Qiagen, Hilden, Germany), according to the manufacturer's instructions. RNA yield and quality were assessed using a NanoDrop spectrophotometer (NanoDrop One, Thermo Fisher

Scientific Inc.). Total RNA concentration was measured using Qubit™ RNA BR Assay Kit and Qubit™ 4.0 Fluorometer (Invitrogen, Thermo Fisher Scientific Inc.). The RNA integrity was assessed using the Agilent 4200 TapeStation System (G2991AA) with the Agilent High Sensitivity.

RNA ScreenTape Assay (Agilent Technologies Inc., Santa Clara, CA, USA). All RNA samples had an RNA integrity number (RIN) ≥ 9 and were considered high-quality samples.

2.5.2. RNA-seq library construction

For RNA-seq library preparation, 300 ng of total RNA per sample were subjected to a ribosomal RNA depletion protocol using the Illumina™ Stranded Total RNA Prep, Ligation with Ribo-Zero™ Plus Kit (Illumina, San Diego, CA, USA). The concentrations of the final libraries were measured using Qubit TM $1\times$ dsDNA HS Assay Kit and Qubit™ 4.0 Fluorometer (Invitrogen, Thermo Fisher Scientific Inc.), and their quality was assessed with Agilent 4200 TapeStation System and Agilent High Sensitivity D1000 ScreenTape Assay (Agilent Technologies Inc.). Libraries were then sequenced on the Illumina NextSeq™ 550 platform (Illumina Inc.) using a NextSeq 500/550 High Output Kit v2.5 (150 cycles, 2×75 bp read length, paired-end) (Illumina Inc.) to achieve sufficient read depth for the analysis.

2.5.3. RNA-Seq bioinformatics

FastQC [27] and MultiQC [28] softwares were used to verify the quality of RNA-Seq data. RSEM computational pipeline [29] was used to quantify the expression of each human gene annotated to Ensembl v100 database [30] and on hg38 reference genome. STAR aligner [31] was used in the alignment step of RSEM pipeline. To filter out the quantified genes that are not really expressed in our model, only genes with a TPM ≥ 1 in at least one sample underwent further analysis, considered to be expressed. Principal component analysis (PCA) plotting was performed using the "prcomp" package of R on the matrix of expression data. DESeq2 [32] was used to define differentially expressed gene (DEGs) with the following thresholds $|log2FC| > 1$ and p.adj < 0.01. Heatmaps showing unsupervised hierarchical clustering of genes were produced using the "pheatmap" function in package of R. Functional analysis of DEGs was performed using Metascape [33] with default parameters and also using QIAGEN IPA software (QIAGEN Inc., https://www.qiagen.com/usproducts/discovery-and-translational-research/next-generation-sequencing/informatics-anddata/interpretation-content-databases/ingenuity-pathway-analysis/). Selected IPA pathways were filtered using -log(p-value) > 3. Moreover, to find Gene Ontology (GO) terms associated with the upstream regulators detected by the IPA analysis in the comparison of "P" versus "D", the list of upstream regulators was filtered to select only the "transcription regulator" molecules, with a p-value <0.001 and associated target molecules in dataset ≥ 5. The resulting list of genes was then annotated with ToppGene Suite [34] with default parameters, and the resulting GO terms were filtered using a p-value adjusted with Bonferroni Correction <0.001. Semantic Plot was produced using Revigo [35] with "*Homo Sapiens*" as species.

3. Results

3.1. 3D trabecular, bone-like tissues

The first step in developing functional trabecular bone-like tissues is efficient cell seeding that comprises adequate cell density and distribution. After 21 days of cultivation in static culture and under bone-like mechanical stimulation, the cell-PLA scaffold interaction exhibited variations among the three cell seeding methods. The live/dead cell assay showed no differences between the three cell seeding methods in terms of cell viability (around 90 % viability) due to the abundance of green fluorescence and the absence of red fluorescence. The absence of red fluorescence does not indicate that no cell loss occurred, and instead may suggest that dead or detached cells were shed during the 21 days of culture. However, there were considerable differences in cell

morphology, infiltration, and distribution between the three cell seeding methods as shown by the live/dead assay and SEM analysis. In detail, suspension seeding resulted in the concentration of cells on one side of the PLA scaffold. In static culture the cells tended to accumulate at the bottom side of the scaffold, since the cell suspension flowed downward due to gravity; whereas, in dynamic culture the media flowed from the bottom to the top of the scaffold, and as a result, the cells were forced to concentrate on the top side of the scaffold (Fig. S1). An alternative approach to increasing the efficiency of static seeding is the use of hydrogels, and in this case, the choice of the hydrogel is of utmost importance. In our work, cell-releasing 2 % alginate caused nonuniform distribution and infiltration of cells throughout the scaffolds. Moreover, cells were preserved inside the hydrogel, maintained their round morphology, and had limited direct interaction with the scaffold as evidenced by the live/dead assay and SEM analysis (Fig. S1). The second hydrogel tested in our work was cell-releasing 0.5 % collagen that exhibited optimal cell distribution and infiltration on multiple focal planes of the scaffold both under direct, unidirectional perfusion and in static culture. As shown in Fig. 2A, the live/dead assay revealed that cells were evenly distributed both at the bottom and top of the scaffolds. Additionally, cells were detected at various depths within the scaffold, including shallow depths (associated with the low zeta stack) and deep depths (associated with the high zeta stacks). The SEM analysis further supported these observations, since cells were able to spread and attach across the entire scaffold, as depicted in Fig. 2B. Exploring novel cell seeding methods should be done while keeping in view cell density as a crucial factor in bone regeneration. Previous studies showed that a high cell seeding density is more advantageous for bone formation and the clinical application of BTE, which supports our choice of a cell seeding density of 3×10^6 cells per scaffold. Therefore, biomimetic PLA scaffold seeded with 3×10^6 cells BM-MSCs using 0.5 % collagen was chosen as the trabecular bone-like tissue model and was used in the following experiments.

3.2. The set-up of cell culture conditions

Following the selection of the cell seeding method, the trabecular bone-like tissues were cultured for 21 days in OM or in BM in static culture (control) or under direct, unidirectional perfusion with or without PEMF stimulation to select the cell culture medium that enables the detection of the response of BM-MSCs to the biophysical stimulation provided as PEMF. The expression levels of COL1A1, OPN, OCN and RUNX2 as the osteogenic marker genes and COL2A1 as the chondrogenic marker gene were relatively quantified by RT-qPCR.

For cells cultured in OM, the results showed that direct, unidirectional perfusion without and with PEMF stimulation induced only a slight upregulation in COL1A1 (~0.7 and 1.2-fold change, respectively), OCN (~1.5-fold change for both conditions), RUNX (~0.8 and 1.0-fold change, respectively), and COL2A1 (~1.7-fold change for both conditions) but not in OPN (~0.07 and 0.1-fold change, respectively), compared to static culture (Fig. 3A). The ratio of COL1A1 to COL2A1 (COL1A1/COL2A1), defined as an index of osteogenic differentiation, was slightly higher with PEMF stimulation in OM (Fig. 3C). For cells cultured in BM and also in comparison with static culture, the results showed that direct, unidirectional perfusion without PEMF stimulation induced only a slight upregulation in COL1A1 (~1.2-fold change), OCN (~1.0-fold change), RUNX2 (~1.4-fold change) and COL2A1 (~0.3-fold change), but not in OPN (~0.09-fold change). However, direct, unidirectional perfusion with PEMF stimulation induced a notable upregulation in COL1A1 (~5.2-fold change) and OPN (~12.0-fold change) and a slight upregulation in OCN (~1.6-fold change), RUNX2 (~2.5-fold change), and COL2A1 (~0.7-fold change), compared to static culture (Fig. 3B). The ratios of COL1A1 to COL2A1 (COL1A1/COL2A1) were higher in BM in comparison to those in OM. Moreover, in BM, the ratio of COL1A1 to COL2A1 (COL1A1/COL2A1) was considerably higher in the presence of PEMF stimulation in comparison to the absence of PEMF

stimulation (Fig. 3C).

Considering the RT-qPCR results, we may propose that PEMF stimulation notably potentiates the osteogenic commitment of BM-MSCs only in the absence of biochemical stimuli supplied by the OM, suggesting that the biochemical stimuli can obscure the role of PEMF stimulation in osteogenic differentiation. That being the case, BM rather than OM was used in the following experiments, and it must be emphasized that the absence of biochemical cues for osteogenic differentiation can better reflect the bone tissue physiology.

3.3. Transcriptomic studies of PEMF stimulation

Following the selection of the cell seeding method and the culture medium, the trabecular bone-like tissues were cultured for 21 days in BM in static culture (control) or under direct, unidirectional perfusion with or without PEMF stimulation for RNA-Seq. The RNA-Seq is a powerful tool for studying gene expression in response to PEMF stimulation by identifying the DEGs. It also aids in studying gene regulation by detecting the transcription factors that are activated or inhibited in response to PEMF. Moreover, the pathway analysis tools aid in identifying the signaling pathways that are activated or inhibited in response to PEMF. Together, these data can provide insights into the molecular mechanisms underlying cellular responses to PEMF stimulation.

#### 3.3.1. Read processing, alignment, and quantification

The high throughput screening (HTS) quality control (QC) is summarized in Fig. S2. Fig. S2A shows that all samples had a read depth of 29 million paired-end reads on average. Fig. S2B shows that the average of the Phred-scaled quality score of each nucleotide in all the reads was >34 in all the samples. Also, no adapter sequences were found in the raw reads, so trimming was not necessary. The reads were subsequently aligned against the human reference genome hg38 and a quantification of every expressed gene was obtained, where expressed gene were defined as those with transcripts per million (TPM) > 1 in at least one sample, as described in the "Methodology Section 2.5".

Furthermore, the inter-group and intra-group variabilities of the expressed genes were assessed by clustering the samples via the principal component analysis (PCA). The results that are presented in Fig. S2C revealed the transcriptomes of the three distinct groups, which are "S", "D", and "P", formed separate clusters, whereas the transcriptomes of the biological replicates of each group cluster tightly. These two observations indicate that the replicates are more highly correlated within samples than between samples.

The differential expression analysis of the three comparisons ("D" versus "S", "P" versus "S", and "P" versus "D") detected changes in the expression levels of 368 genes in "D" versus "S", 654 genes in "P" versus "S", and 224 genes in "P" versus "D", which summed up to a total of 956 unique DEGs (Fig. 4). These DEGs were defined using $|\log_2 FC| > 1$ and p.adj < 0.01 as statistical cut-offs, as described in the "Methodology Section 2.5". The complete tables reporting log2FC and adjusted *p*-value of the DEGs in each comparison are provided as a supplementary file 1. Moreover, the complete tables reporting the upstream regulators that were filtered to select only the "transcription regulator" molecules with a p-value <0.001 and associated target molecules in the dataset ≥5 are provided as a supplementary file 2.

To gain biological insights from these lists of DEGs, further analyses were performed. For the sake of explicating the results obtained by the transcriptomic studies in a concise and explicit manner, we focused our attention on the changes in the expression levels of genes and upstream regulators related to bone regeneration on one hand, and to some of the previously reported biological effects of PEMF stimulation on the other. The latter was done using QIAGEN IPA, as described in the "Methodology Section 2.5". The identified DEGs were first used to identify the signaling pathways that are affected by PEMF stimulation, and second, to identify the upstream regulators that are affected by PEMF stimulation. The identified upstream regulators then underwent pathway
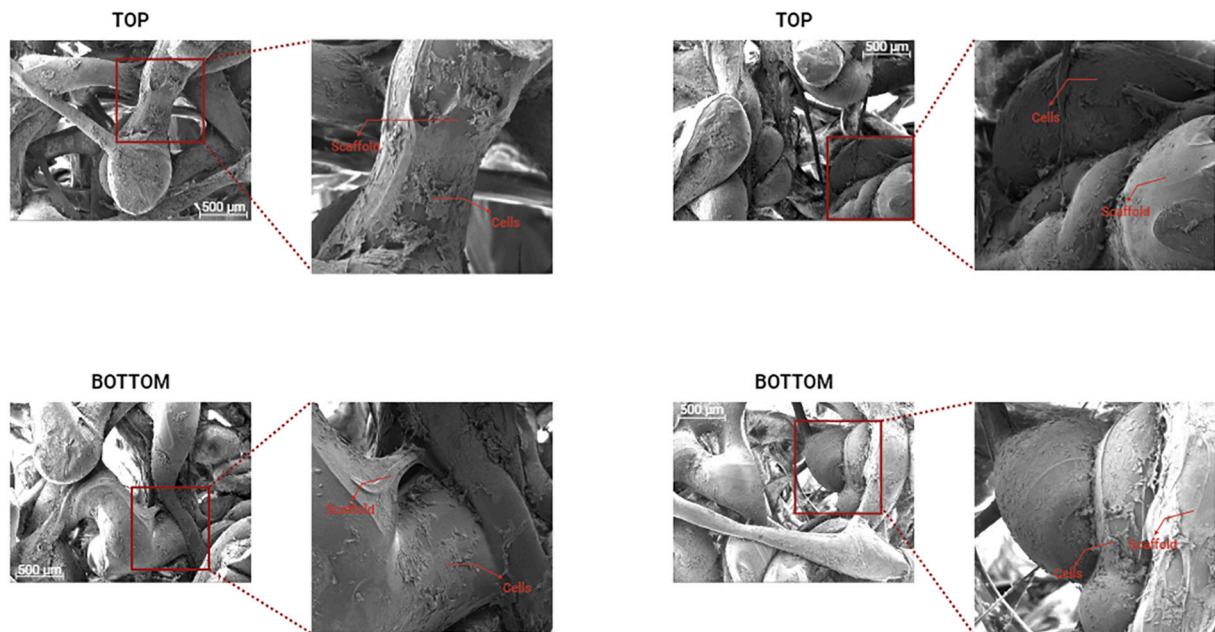
A
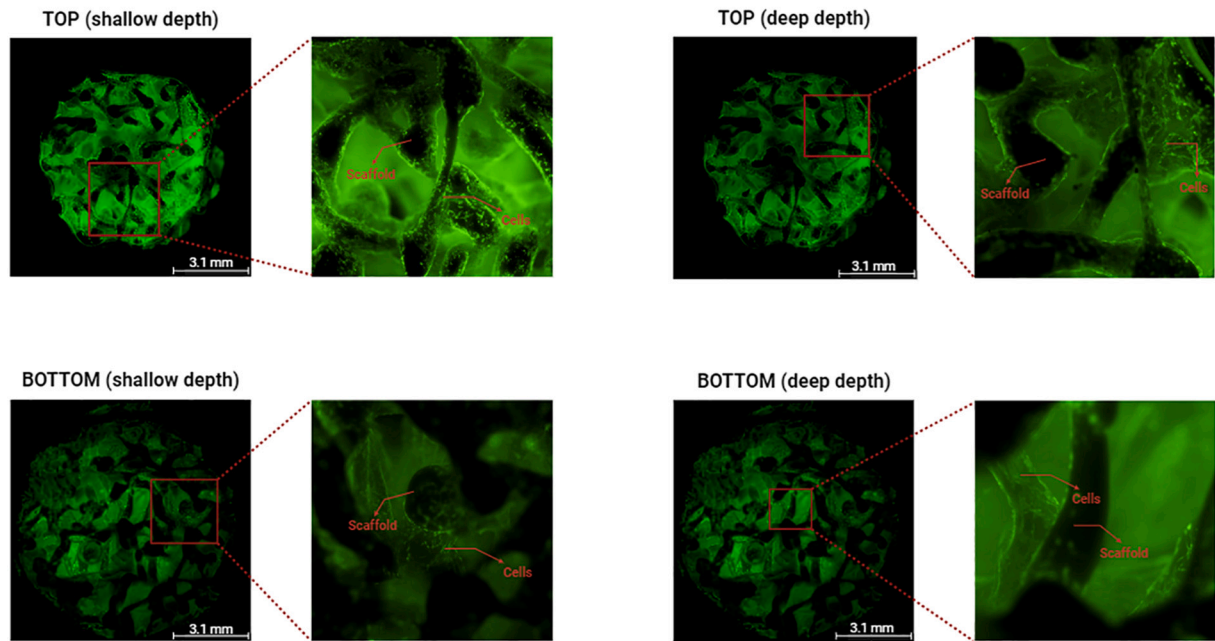
B

Fig. 2. Live/dead cell assay and scanning electron microscope (SEM) analysis of trabecular bone-like tissues cultured for 21 days in an automated perfusion bioreactor. **(A)** Representative calcein-AM/EthD-1 images of bone marrow-derived mesenchymal stem cells (BM-MSCs) seeded on polylactic acid (PLA) scaffolds via cell-releasing 0.5 % collagen. Images represent the upper and lower sides of the scaffold and focal planes with shallow and deep depths. Images were taken with 5× magnification; scale bars correspond to 3.1 mm. **(B)** SEM images of BM-MSCs seeded on PLA scaffolds via cell-releasing 0.5 % collagen. Images represent the upper and lower sides of the scaffold. Images were taken with 50× magnification; scale bars correspond to 500 μm.
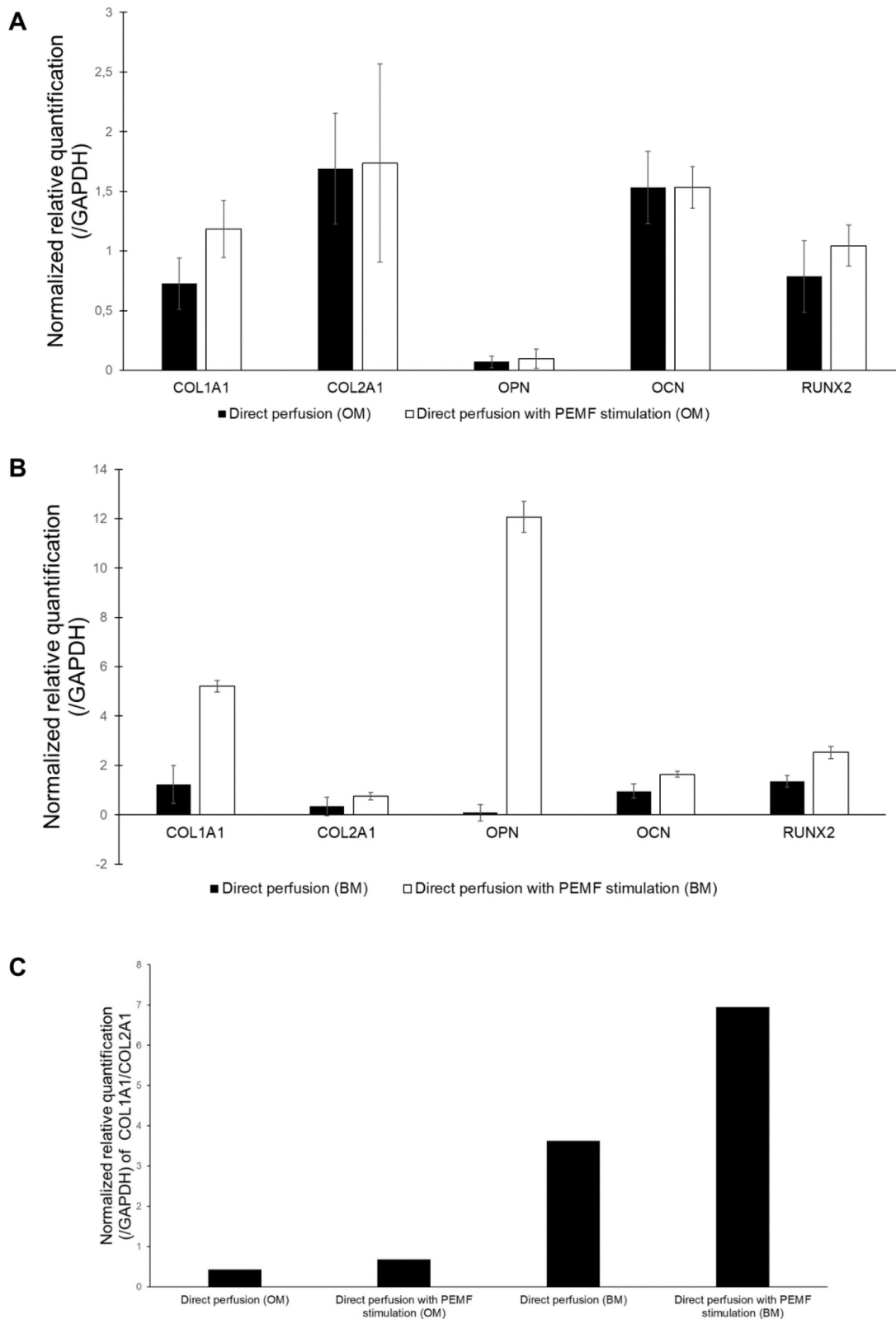
Fig. 3. Gene expression analyses of bone marrow-derived mesenchymal stem cells (BM-MSCs) in the trabecular bone-like tissues after 21 days of culture. The osteogenic and chondrogenic mRNA expression in BM-MSCs cultured under direct, unidirectional perfusion without and with pulsed electromagnetic field (PEMF) stimulation in comparison with static culture in (**A**) osteogenic medium (OM) and (**B**) basal medium (BM). The relative expressions of collagen type I alpha 1 chain (COL1A1), osteopontin (OPN), osteocalcin (OCN), runt-related transcription factor 2 (RUNX2), and collagen type II alpha 1 chain (COL2A1) mRNAs were analyzed by reverse transcription-quantitative PCR (RT-qPCR) and were calculated by $2^{-\Delta\Delta CT}$ method with normalization to the levels of GAPDH. Bars represent the mean fold change of three biological replicates $\pm$ standard error of the mean (SEM). (**C**) The ratio of COL1A1 to COL2A1 (COL1A1/COL2A1) of BM-MSCs cultured in OM and BM.

A

N = 956

B

D vs. S
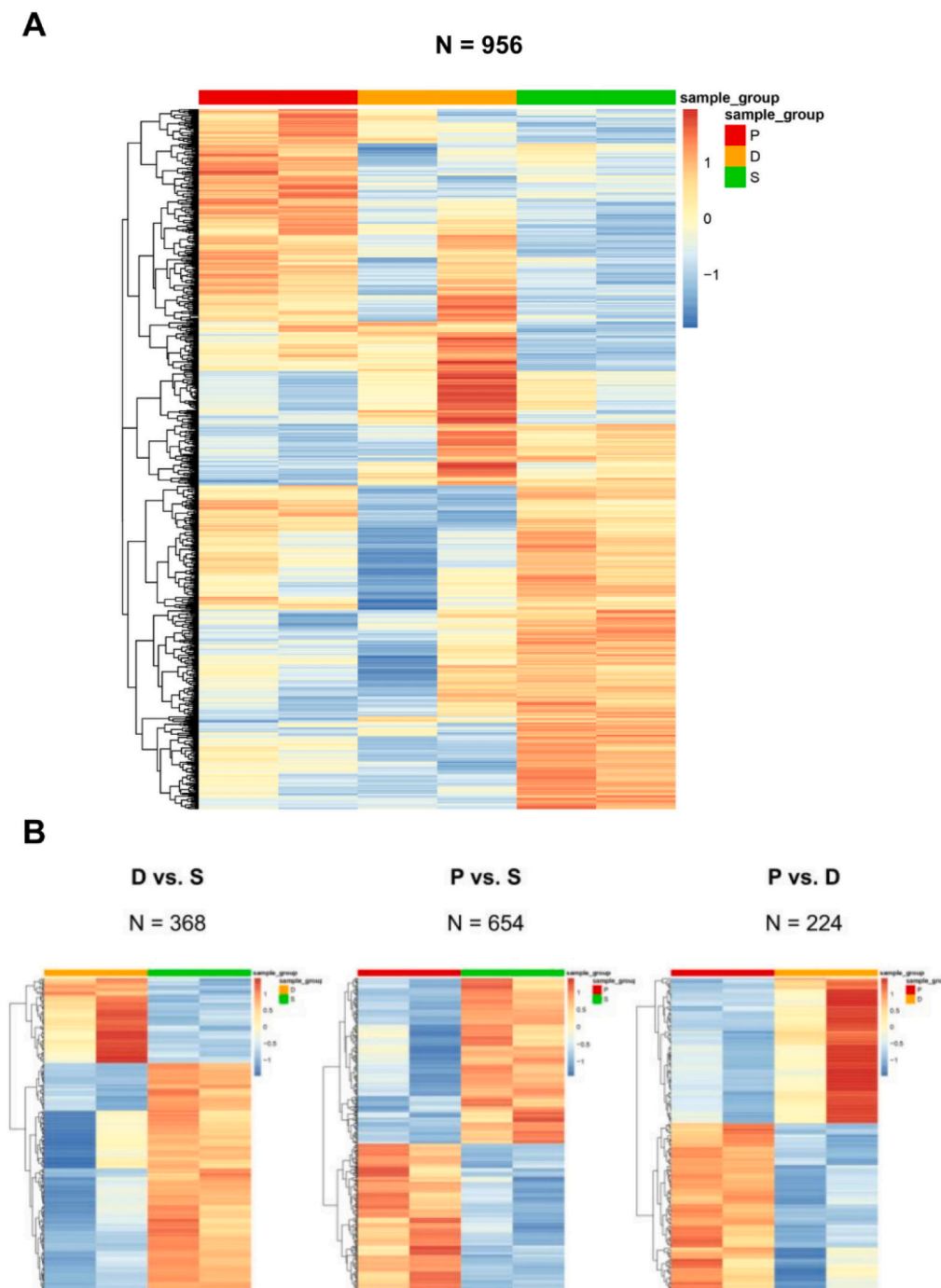
N = 368

P vs. S

N = 654

P vs. D

N = 224

Fig. 4. Heatmaps of differentially expressed gene (DEGs) of bone marrow-derived mesenchymal stem cells (BM-MSCs) cultured in basal medium for 21 days. **(A)** Heatmap of all DEGs in each of the three groups ("S", "D", and "P"). **(B)** Heatmaps of DEGs in the three comparisons ("D" versus "S", "P" versus "S", and "P" versus "D"). "S" represents static culture, "D" represents direct, unidirectional perfusion, and "P" represents direct, unidirectional perfusion with PEMF stimulation.

enrichment analysis to identify the pathways that are regulated by the identified upstream regulators and the genes that are involved in the pathways. Furthermore, we only included the results obtained for the comparison of "P" versus "D" since the principal objective of our study was to track down the signaling pathways targeted by PEMF stimulation in an in vitro environment resembling as closely as possible the physiological environment of bone tissue.

3.3.2. Immune potential of PEMF stimulation

Bone healing involves multiple phases that overlap, and these are the inflammatory phase, fibrovascular phase, bone formation phase, and

bone remodeling phase. The acute inflammatory phase is known to facilitate normal bone healing, and as such, inhibition of inflammation and chronic inflammation are associated with delays and impairments in bone healing, respectively [36].

The GO enrichment analysis of the DEGs in the comparison of "P" versus "D" using Metascape (Fig. S3) showed that the signaling pathways evoked by PEMF stimulation and implicated in the first phase of bone healing are: GO:0006954 (inflammatory response), R-HSA-1280215 (cytokine signaling in immune system), GO:0001819 (positive regulation of cytokine production), WP5055 (burn wound healing), GO:0002697 (regulation of immune effector process), and R-HSA-

6798695 (neutrophil degranulation). The analysis of DEGs in the comparison of "P" versus "D" using QIAGEN IPA (Fig. 5) revealed additional signaling pathways, which are: mammalian target of rapamycin (mTOR) signaling (enriched only), macrophage classical activation signaling pathway (activated), antigen presentation pathway (enriched only), pathogen-induced cytokine storm signaling pathway (activated), Th1 pathway (activated), Th2 pathway (enriched only), MSP-RON signaling in macrophages pathway (deactivated), Th1 and Th2 activation pathway (enriched only), IL-12 signaling and production in macrophages (deactivated), wound healing signaling pathway (activated), macrophage alternative activation pathway (activated), and neuroinflammation signaling pathway (activated). The pathway enrichment analysis of the upstream regulators highlighted positive regulation of immune system process, response to wounding, and positive regulation of cytokine production (Fig. 6B).

3.3.3. Angiogenic potential of PEMF stimulation

With regards to the second stage of bone healing, the fibrovascular phase [36], the GO enrichment analysis in the comparison of "P" versus "D" using Metascape (Fig. S3) highlighted GO:0001944 (vasculature development), GO:0003013 (circulatory system process), GO:0060840 (artery development), and WP3888 (vascular endothelial growth factor A-vascular endothelial growth factor receptor 2 (VEGFA-VEGFR2) signaling) as signaling pathways promoted by PEMF. The analysis of DEGs in the comparison of "P" versus "D" using QIAGEN IPA (Fig. 5) did not identify signaling pathways associated with angiogenesis. However, the identified upstream regulators included VEGFA, transforming growth factor beta 2 (TGFB2), fibroblast growth factor 2 (FGF2), fibroblast growth factor receptor 1 (FGFR1), and some members of the mitogen-activated protein kinase (MAPK) signaling pathway, which are MAPK1, MAPK3, and MAPK14 (Fig. 6A). The pathway enrichment analysis of the upstream regulators highlighted the regulation of vasculature development (Fig. 6B).

3.3.4. Osteoinductive potential of PEMF stimulation

The final phases of bone healing are the bone formation and bone remodeling phases [36]. Since the preliminary gene expression analyses

revealed that only when bone-like mechanical stimulation was coupled with PEMF the upregulation in the osteogenic marker COL1A1 became significant, the transcriptomic studies served the purpose of clarifying the osteoinductive potential of PEMF stimulation.

The GO enrichment analysis of the DEGs in the comparison of "P" versus "D" using Metascape showed that PEMF stimulation evoked GO:0001501 (skeletal system development) with the main TFs involved being β-catenin 1 (CTNNB1) and nuclear factor kappa B (NF-κB) inhibitor alpha (NFKBIA) (Fig. S3). By contrast, the analysis of DEGs in the comparison of "P" versus "D" using QIAGEN IPA (Fig. 5) did not identify signaling pathways associated with osteogenesis, but as in the case of angiogenesis, the related upstream regulators should be acknowledged, and these are: members of the canonical Smad-dependent signaling pathway of the transforming growth factor (TGF)-β/bone morphogenetic protein (BMP) signaling, which are BMP2, BMP7, SMAD1, and SMAD3; members of the non-canonical-Smad-independent signaling pathway of the TGF-β/BMP signaling (that is, p38 mitogen-activated protein kinase/p38 MAPK) including P38 MAPK; members of the WNT/β-catenin signaling pathway including CTNNB1 and WNT3A (predicted by IPA, but not actually expressed in our samples); the member of the NF-κB signaling pathway that is NFKBIA; as well as the runt-related transcription factors (RUNX) including RUNX2 (Fig. 6A). The pathway enrichment analysis of the upstream regulators highlighted regulation of osteoblast differentiation, ossification, and regulation of WNT signaling pathway (Fig. 6B).

3.3.5. Secondary pathways altered by PEMF stimulation

As the present work aimed to explore the biological effects of PEMF stimulation using an innovative bioreactor-based investigation platform, the results obtained by the transcriptomic studies were thoroughly examined. Not surprisingly, the biological effects of PEMF have gone beyond bone healing and in this section, we presented a few of the biological effects of PEMF stimulation that were investigated by previous studies.

To start with, the possible role of PEMF stimulation in initiating epigenetic alterations was checked, especially that this role called attention recently. Cited as an example, the work by De Mattei et al.
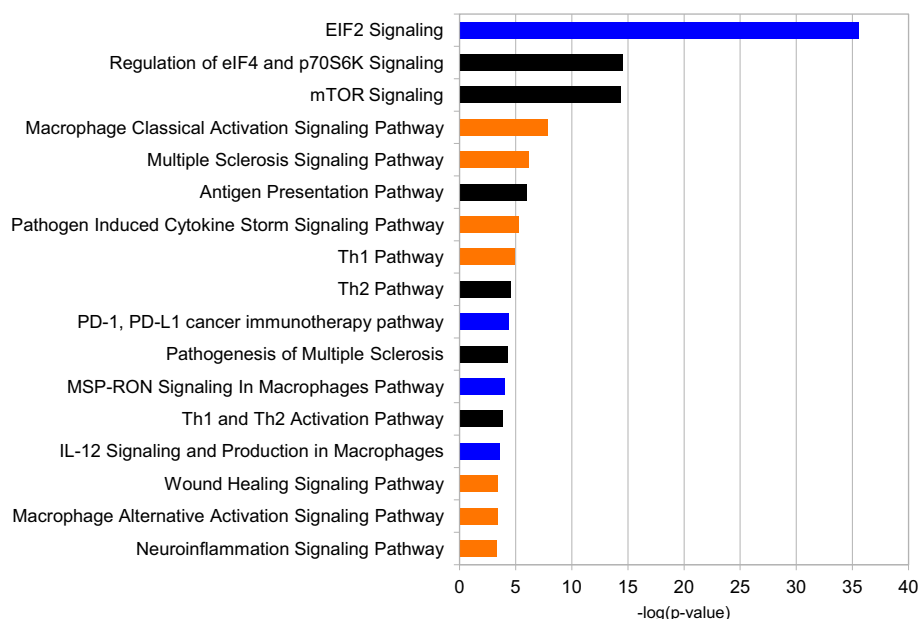

Fig. 5. Bar plot representing selected enriched pathways from QIAGEN Ingenuity Pathway Analysis (IPA) of differentially expressed genes (DEGs) in the comparison of "P" versus "D", where "D" represents direct, unidirectional perfusion and "P" represents direct, unidirectional perfusion with PEMF stimulation. Orange bars represent activated pathways in "P" in comparison with "D"; Blue bars represent deactivated pathways in "P" in comparison with "D"; Black bars represent pathways that were only enriched in "P" in comparison with "D". (For interpretation of the references to colour in this figure legend, the reader is referred to the web version of this article.)
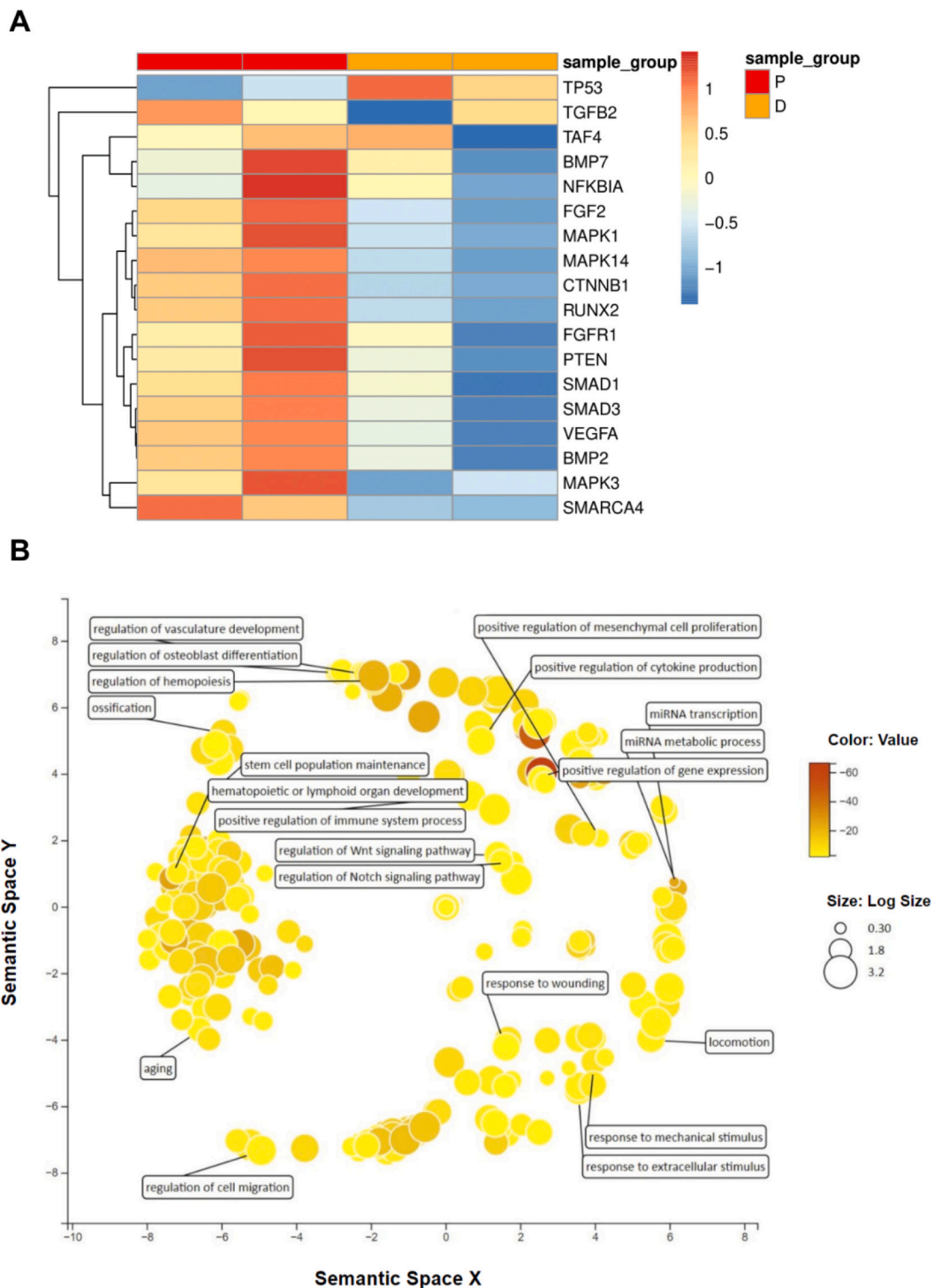
Fig. 6. Upstream regulators detected on QIAGEN Ingenuity Pathway Analysis (IPA) of the comparison of "P" versus "D", where "D" represents direct, unidirectional perfusion and "P" represents direct, unidirectional perfusion with PEMF stimulation. (A) Heatmap of the upstream regulators that were differentially expressed. (B) Pathway enrichment analysis of the upstream regulators using Revigo.

(2020) presented that PEMF stimulation can modulate miRNAs involved in osteogenesis and angiogenesis, mainly miR26a and miR29b [37]. In the current study, the pathway enrichment analysis of the upstream regulators highlighted miRNA transcription and miRNA metabolic process (Fig. 6B). Therefore, a deeper insight into the biological significance of these epigenetic alterations can present a great topic for future research.

Moreover, the first signaling pathway that was primarily underlined by the analysis of DEGs in the comparison of "P" versus "D" using IPA,

that is the eukaryotic Initiation Factor 2 (eIF2) (deactivated), refocused the attention on the possible modifications in gene expression of human BM-MSCs that can be triggered by exposure to PEMF. eIF2 is known to play a central role in the integrated stress response (ISR), an adaptive signaling pathway required for the maintenance of cellular homeostasis by reducing protein synthesis, while allowing the translation of a set of mRNAs encoding transcription factors and other proteins [38]. The modified signaling pathways and downstream events involved in gene expression were searched for, and included the regulation of eIF4 and

p70S6K signaling (enriched only) (Fig. 5), and the upstream regulators comprised SWI/SNF related, matrix associated, actin dependent regulator of chromatin, subfamily a, member 4 (SMARCA4) and TATA-box binding protein associated factor 4 (TAF4), among others (Fig. 6A). The pathway enrichment analysis of the upstream regulators highlighted positive regulation of gene expression (Fig. 6B). These data can support the hypothesis that PEMF perpetrated its functions by directly altering gene expression, from transcription and translation to epigenetics.

Another utility of PEMF stimulation that was previously described by various studies is its potential use in certain pathological conditions with the intention of ameliorating the pathogenesis of these conditions. The pathological conditions that were detected in the present study include multiple sclerosis (MS) and tumor. For MS, the analysis of DEGs in the comparison of "P" versus "D" using QIAGEN IPA (Fig. 5) highlighted MS signaling pathway (activated) and pathogenesis of MS (enriched only), and this desirable outcome of PEMF was detected by various studies that explored the effects of PEMF on spasticity [39]. Besides MS, biophysically stimulated BM-MSCs exhibited tumor suppression properties, and the analysis of DEGs in the comparison of "P" versus "D" using QIAGEN IPA (Fig. 5) included PD-1, PD-L1 cancer immunotherapy pathway (deactivated), in addition to the expression of the upstream regulators TP53 and phosphatase and tensin homolog (PTEN) that are known tumor suppressors (Fig. 6A).

3.4. Validation of raw expression signals and differential gene expression

To further investigate the signaling pathways that were reported by previous studies as potential pathways targeted by PEMF and to validate the results obtained by the transcriptomic studies, gene expression analyses were performed. Accordingly, the changes in the relative expression levels of certain mRNAs from all three groups ("S", "D", and "P") were tracked down for the validation of the raw expression signals (Fig. S4) and for the validation of the DEGs (Fig. S5).

Here we present the outcomes of the gene expression analyses obtained for the comparison of "P" versus "D" in order to compare them with the outcomes of the transcriptomic studies (Fig. S4C). Starting with signaling pathways, the relative expression levels of $A_{2A}AR$, $A_{2B}AR$, and A_3AR mRNAs were detected to examine adenosine signaling as it is extensively reported in the literature, but was not highlighted by the transcriptomic studies of our study. While $A_{2A}AR$ and $A_{2B}AR$ were slightly upregulated (~1.0 and 0.6-fold change, respectively) due to PEMF stimulation, A_3AR was not. Another signaling pathway that is highly noted by previous works is the Wnt/β-catenin signaling pathway with WNT1 being the mainly reported member. The relative expression level of WNT1 mRNA showed that WNT1 was not expressed by BM-MSCs, even after PEMF stimulation. This finding is in line with the results of the transcriptomic studies, since CTNNB1 and WNT3A (predicted by QIAGEN IPA, but not actually expressed in our samples), and not WNT1, were the identified members of the WNT/β-catenin signaling pathway. To get additional information on the epigenetic alterations caused by PEMF, the relative expression level of the most commonly reported epigenetic modulator in the literature, that is miR26A1, was evaluated, and results showed that PEMF caused a slight elevation in the expression of miR26A1 (~1.0-fold change), and this was also verified by transcriptomic studies that highlighted other miRNAs, and not miR26A1, as major epigenetic players.

To corroborate the biological effects of PEMF on the cellular level, the relative expression levels of the osteogenic markers, angiogenic markers, and chondrogenic markers were traced. The outcomes showed higher expression of RUNX2, OCN, and OPN mRNAs with PEMF stimulation in comparison with perfusion alone (~1.9, 1.7, and 147.7-fold change, respectively), and similar tendencies were seen with the mRNAs of the angiogenic markers ICAM1, PECAM1, and KDR (~1.9, 13.7, and 1.1-fold change, respectively) and the mRNA of the chondrogenic marker SOX9 (~2.5-fold change). Based on the results, we can

hypothesize that PEMF stimulation tends to preserve the ability of BM-MSCs to differentiate into various cell types. This is because both osteogenic and angiogenic markers were upregulated. This property is a key characteristic of stem cells, which are known for their ability to differentiate into different cell types.

4. Discussion

Developing an *in vitro* biomimetic investigation platform for bone biology research that mimics, as closely as possible, the architectural and mechanical environment of bone requires joining some key pillars. The first step in developing functional trabecular bone-like tissues is efficient cell seeding that comprises cell density and distribution. The results we obtained with the three cell seeding methods that we evaluated (suspension seeding, cell-releasing 2 % alginate, and cell-releasing 0.5 % collagen) are in line with previous findings. Static seeding of cells in liquid suspension was previously tested by Cámara-Torres et al. (2020), who altered the viscosity and density of the culture medium using dextran and Ficoll, respectively, and proved that increasing the viscosity and the density of the culture medium did not only cause homogeneous cell infiltration of BM-MSCs into the 3D scaffolds prepared from the copolymer poly(ethylene oxide terephthalate)/poly(butylene terephthalate) (PEOT/PBT), but also improved osteogenesis [40]. Moreover, the superiority of collagen to alginate in our study emphasizes the utility of collagen for cell seeding that has been evaluated by various studies. One of which is the work of Fahimipour et al. (2019), who fabricated a bone ECM-mimetic matrix composed of heparin-functionalized collagen and immobilized bone morphogenetic protein 2 (BMP2) to seed dental pulp MSCs into β-tricalcium phosphate (β-TCP) scaffolds, and they revealed that the collagen-heparin matrix maintained the bioactivity of BMP2, enhanced the cell seeding efficiency, and supported osteogenesis [41]. Concerning our adherence to high-density seeding, this choice is supported by several studies including those of Hsieh et al. (2019) [42] and Wu et al. (2015) [43] who verified the superiority of high cell seeding density.

The second step in developing an in vitro investigation platform that is targeted for assessing the effects of PEMF on BM-MSCs in the presence of bone-like mechanical environment is the selection of the cell culture conditions. We aimed to compare BM with OM in terms of cellular and molecular changes caused by mechanical and biophysical stimulation. In our study, we observed that there exists a subtle association between direct perfusion and the osteogenic differentiation of BM-MSCs. This correlation was evident in BM but not in OM, since the ratio of COL1A1 to COL2A1 (COL1A1/COL2A1) exhibited a slight inclination towards osteogenic differentiation. However, other authors have succeeded in highlighting the positive influence of biomechanical stimuli on osteogenesis. Lim et al. (2019) were able to design a fully automated bioreactor system (fABS) and to induce proliferation, osteogenesis, and chondrogenesis of human BM-MSCs in a water-jacketed culture chamber (WJCC) via shear stress of 1.018×10^{-6} Pa even in the presence of the biochemical stimuli [44]. Moving towards more complex applications of bioreactors, Vetsch et al. (2017) aimed to use a perfusion bioreactor that specifically mimics the mechanical environment during early fracture healing or during bone remodeling, which corresponds to v = 0.001 m/s and v = 0.061 m/s, respectively. In this respect, they utilized human BM-MSCs, 3D silk fibroin scaffolds, and an osteogenic medium, and showed that by using two different flow rates the cell fate was directed towards either proliferation or osteogenic differentiation [45]. In earlier work, also employing a 3D cell culture and human BM-MSCs, Bjerre et al. (2008) cultivated silicate-substituted tricalcium phosphate (Si-TCP) scaffolds in a perfusion bioreactor using media supplemented with 10^{-8} M 1,25-(OH)$_2$-vitamin D$_3$; and again, in this case, the authors managed to observe enhanced proliferation, osteogenic differentiation, and cell/matrix deposition at a flow rate of 0.1 mL/min [46]. The dissimilar outcomes of the perfusion bioreactors in BTE can be attributed to the alterations in experimental conditions related to the bioreactor

systems since they are operated with unique experimental configurations, as well as to the scaffold material, scaffold properties, cell type, and cell culture duration, in addition to environmental conditions. Therefore, results obtained from bioreactor systems can be compared only when identical, standardized bioreactor systems are used under the same experimental and environmental conditions, as was previously demonstrated by Zhao et al. (2018) [47] and other researchers. However, in our study, we were able to demonstrate the osteogenic potential of PEMF stimulation using our bioreactor-based investigation platform with BM rather than OM. Previous in vitro studies also proved possible the role of PEMF stimulation in bone regeneration. Starting from studies on 2D cell cultures, Ongaro et al. (2014) revealed that both human BM-MSCs and adipose-derived mesenchymal stem cells (AD-MSCs) exposed to continuous PEMF stimulation (1.5mT, 75 Hz) for 28 days in osteogenic medium and in the absence or presence of BMP2 promoted osteogenic differentiation [48], and Kang et al. (2013) were also able to show similar outcomes using PEMF stimulation (30/45Hz, 1mT) for 8 h per day for up to 20 days [49]. On a similar note, previous studies by Jansen et al. (2010) [50], Sun et al. (2010) [51], and Tsai et al. (2009) [52] reported enhanced osteogenesis owing to PEMF stimulation. Conversely, other studies on PEMF stimulation using 2D cell cultures, such as the ones performed by Kaivosoja et al. (2012) [53] and Yan et al. (2010) [54] were incapable of verifying the osteoinductive properties of PEMF. Yet, the response of cells to external stimuli varies significantly between 2D and 3D cell cultures, and the latter was amply shown by the study performed by Schwartz et al. (2009) [55]; thus, the evaluation of PEMF's biological outcomes should be compulsory done on 3D cell cultures [56]. The few studies on PEMF stimulation and 3D cell cultures involve titanium, calcium phosphate scaffolds, and polymers, as described previously by Galli et al. [10] One of the most recent works on titanium by Broise et al. (2018) involved nanostructured TiO_2, where human BM-MSCs were seeded on the scaffolds, cultured in osteogenic medium, and exposed to PEMF stimulation (2 mT, 75 Hz) for 10 min per day for a total of 28 days. The authors showed that PEMF can have a significant osteoinductive potential that involves selective calcium-related osteogenic pathways [57]. One of the latest studies employing calcium phosphate scaffolds, which was performed by Schwartz et al. (2008), did not achieve comparable results as the authors were unable to demonstrate that PEMF stimulation enhances the osteogenic effects of BMP2 on human BM-MSCs cultured in osteogenic medium [58]. Ultimately, among the recent work on polymers, poly(caprolactone) (PCL) nanofibrous scaffolds and human AD-MSCs were cultured in basal medium or osteogenic medium for up to 21 days by Arjmand et al. (2017), who were able to show that PEMF stimulation alone has an osteoinductive potential similar to that of osteogenic medium [59]. By this stage, the osteoinductive potential of perfusion bioreactors and PEMF was examined separately, and as previously described, mimicking in vitro the bone tissue-specific environment is a central factor in bone biology research. Thus far, only a limited number of studies examined PEMF as part of an in vitro bone tissue experimental model encompassing 3D cell cultures and perfusion bioreactors. The latest work by Wang et al. (2019) evaluated EMF (15Hz, 1 mT) exposure for 4h per day in vitro using hydroxyapatite/collagen type I (HAC) scaffolds and rabbit BM-MSCs in basal and osteogenic media, as well as in vivo by implanting the obtained cell-laden constructs in a rabbit femur condyle defect model, and the obtained results showed that EMF ameliorated bone regeneration and bone integration [60]. The desirable outcomes of PEMF on bone cells using 3D cell cultures and perfusion bioreactors were also highlighted by Tsai et al. (2007) via poly(dl-lactic-*co*-glycolic acid) (PLGA) scaffolds and rat osteoblasts [61]. Although none of these platforms entirely replicate the bone tissue-specific environment, they represent a more legitimate tool for bone biology research.

After selecting the optimal trabecular, bone-like tissue and culture condition, the DEGs identified by transcriptomic studies were analyzed to identify the signaling pathways and upstream regulators altered by PEMF stimulation by comparing the culture conditions "P" and "D".

Moreover, the identified upstream regulators underwent pathway enrichment analysis. Starting with the first phase of bone healing, our results showed that in the absence of a pathological state, such as bone fracture, PEMF has an immune potential as it stimulates the immune properties of human BM-MSCs and can therefore modulate the immune system. This outcome is consistent with the findings of previous studies that presented the anti-inflammatory properties of PEMF. However, it is worth noting that most in vitro studies performed to date were done on 2D cell cultures and in the presence of an inflammatory state, and only a few of them investigated MSCs. For instance, synovial fibroblasts from OA patients were exposed to PEMF by Ongaro et al. (2011), who showed that EMF predisposed an anti-inflammatory state via the activation and upregulation of the adenosine receptors A_{2A} and A_3, the inhibited release of prostaglandin E_2 (PGE₂) and other proinflammatory cytokines, and finally, the elevated release of anti-inflammatory cytokines [62]. For the immune potential of PEMF stimulation, several studies suggested the involvement of ARs, and proposed $A_{2A}AR$ and A_3AR as the major players in various cell lines including human neutrophils, synoviocytes, chondrocytes, and osteoblasts [63]. The transcriptomic studies of the present work did not highlight signaling pathways involving ARs; yet, these transmembrane receptors are not the only ones that can be linked to the immune potential of PEMF stimulation. This point was demonstrated by other studies, such as the work done by Ferroni et al. (2018), who studied mTOR signaling pathway in particular, and revealed that human AD-MSCs exposed to PEMF showed increased cell proliferation, cell adhesion, and osteogenic commitment even in inflammatory conditions via mTOR signaling pathway [64]. The involvement of the mTOR signaling pathway was also demonstrated in the transcriptomic studies of the present study, as mentioned above.

The second phase of bone healing, the fibrovascular phase, is also targeted by PEMF stimulation, according to our results. This capacity of PEMF stimulation has been reported by previous in vitro studies too, yet, they were mainly performed on 2D cultures. One example is the recent study by Gerdesmeyer et al. (2022), who used primary human BM-MSCs cultured in osteogenic medium and exposed them to high-intensive PEMF (80–150 mT, 1–3 Hz) for up to 14 days. The authors showed that only at day 7 of culture PEMF with a magnetic field strength of 80 mT caused an increase in the released proangiogenic factor VEGF, while it did not upregulate the expression of VEGF and pro-osteogenic factors genes [65]. In previous work in vitro and in vivo, Tepper et al. (2004) also depicted a major role of FGF2 in the angiogenic potential of PEMF [66]. Regardless of the heterogeneity among the examined angiogenic markers, there is substantial evidence of the involvement of the MAPK signaling pathway, with a concrete role of FGF2 in the angiogenic potential of PEMF stimulation. This was also observed in the present study using BM-MSCs, since the transcriptomic studies underlined upstream regulators that are tightly linked to the activation of MAPK signaling pathway and to the regulation of angiogenesis.

Finally, the last phases of bone healing, which are the bone formation phase and bone remodeling phase, are also altered by PEMF stimulation relative to our findings. However, it is noteworthy that regardless of the firm bond between PEMF stimulation and bone healing, the complete mechanisms participating in this action are slightly recognized, and adding to this, the findings of studies are not well defined. In 2D cultures, for instance, Gerdesmeyer et al. (2022) did not observe a significant upregulation in the expression of COL1, ALP, OCN, and BMP2 by human BM-MSCs exposed to PEMF after 7 and 14 days of culture in comparison with cells cultured in the absence of PEMF [65]. Conversely, Wu et al. (2018), using mouse embryonic stem cells exposed to PEMF (0.1–10 mT, 30 Hz), revealed that PEMF induced osteoblastogenesis through increased intracellular Ca^{2+} and the Wnt-Ca^{2+}/Wnt-β-catenin signaling pathway [67]. The effect of PEMF stimulation on bone healing was also tested in 3D cultures. Using calcium phosphate (CaP) surfaces and three different cell lines (human BM-MSCs, human osteoblast-like osteosarcoma MG63 and SaOS-2 cells, and normal human osteoblasts), Schwartz et al. (2009) showed that PEMF stimulation elevated the

expression of the TNF receptor superfamily member 11b (TNFRSF11B), but did not alter that of RANKL, suggesting that PEMF stimulation acts via a signaling pathway other than those that mediate RANKL expression or secretion [55]. The signaling pathways involved in bone metabolism that are mainly correlated with the osteogenic potential of PEMF include TGF-β/BMP signaling [68], WNT/β-catenin signaling [69], and NF-κB signaling [70]. In the present study, members of all three pathways were detected to be upregulated by PEMF stimulation. Alongside this, the single most startling finding is the remarkable upregulation of the expression of OPN caused by PEMF stimulation in comparison with perfusion alone. The latter is worth further investigation, especially that OPN possesses multiple functions and plays roles in inflammation, cardiovascular diseases, cellular viability, cancer, diabetes, and renal stone disease [71].

5. Conclusions

In spite of the advancements in uncovering the biological effects of biophysical stimulation, including PEMF, a comprehensive understanding of the altered signaling pathways is yet to be realized. There is no doubt that in vitro experiments omitting the complexity and peculiarity of tissue types are henceforward deficient, and in parallel, legislations aiming to stop the use of animals for scientific purposes make in vivo experiments an unfeasible alternative. As such, the most propitious substitute is the application of in vitro investigation tools that attempt to replicate the parameters of specific physiological environments as closely as possible. Human mesenchymal stem cells (hMSCs) are sensitive to biomechanical and biophysical stimuli, which means that it is enormously substantial to track down the signaling pathways involved in the stimulus-response transformations resulting from biomechanical and biophysical stimulation.

Based on evidence from the current study, human BM-MSCs cultivated in an in vitro investigation platform replicating the microarchitecture of trabecular bone and the physiological environment of bone tissue can respond to PEMF stimulation by inducing bone healing via the expression of immune, angiogenic, and osteogenic potential. The study also successfully mapped the gene transcripts of human BM-MSCs that are sensitive to biomechanical and biophysical stimulation. Another observation to emerge from this study is the ability of PEMF stimulation to initiate new features in the human BM-MSCs including the aptitude to interfere in certain pathological states. Thus, based on evidence from the present study, the proposed in vitro investigation platform represents a suitable tool for investigating the biological effects of PEMF stimulation.

The current work is a call for other researchers to avail themselves of the opportunity to access the transcriptome profile of human BM-MSCs to direct their future research. It should be emphasized that a lot remains obscured, and more work is needed to discover how different cell types respond to PEMF stimulation, how mechanical stimuli resembling the bone physiological environment affect the biological effects of PEMF, and how the modification of PEMF parameters (amplitude, frequency, pulse shape, and duration of exposure) modify the biological outcome. Our future work will aim to tackle in depth the previously mentioned points. As we discover more about how PEMF stimulation affects our biology, healthcare professionals can use this information to tailor PEMF treatments to individual patients.

Supplementary data to this article can be found online at https://doi.org/10.1016/j.bone.2024.117065.

Funding

CRediT authorship contribution statement

Farah Daou: Writing – review & editing, Writing – original draft, Investigation. **Beatrice Masante:** Resources. **Stefano Gabetti:** Resources. **Federico Mochi:** Resources. **Giovanni Putame:** Resources. **Eleonora Zenobi:** Resources. **Elisa Scatena:** Resources. **Federica Dell'Atti:** Investigation. **Francesco Favero:** Data curation. **Massimiliano Leigheb:** Writing – review & editing. **Costantino Del Gaudio:** Resources. **Cristina Bignardi:** Resources. **Diana Massai:** Writing – review & editing, Conceptualization. **Andrea Cochis:** Writing – review & editing, Conceptualization. **Lia Rimondini:** Writing – review & editing, Supervision, Conceptualization.

Declaration of competing interest

Lia Rimondini reports was provided by University of Eastern Piedmont'Amedeo Avogadro' Department of Health Sciences. Lia Rimondini reports a relationship with University of Eastern Piedmont'Amedeo Avogadro' Department of Health Sciences that includes:. Not applicable. If there are other authors, they declare that they have no known competing financial interests or personal relationships that could have appeared to influence the work reported in this paper.

Data availability

The RNA-Seq data are available in the NCBI GEO with the following ID: GSE231791.

Acknowledgments

References

[1] R.H.W. Funk, T. Monsees, N. Özkucur, Electromagnetic effects – from cell biology to medicine, Prog. Histochem. Cytochem. 43 (4) (Feb. 2009) 177–264, https://doi.org/10.1016/J.PROGHI.2008.07.001.

[2] L. Massari, et al., Biophysical stimulation of bone and cartilage: state of the art and future perspectives, Int. Orthop. 43 (3) (2019), https://doi.org/10.1007/s00264-018-4274-3 (pp. 539–511).

[3] Food and Drug Administration (FDA), ORDP - Bone Growth Stimulators Executive Summary-08.07.20, 2020.

[4] H. Hu, et al., Promising application of pulsed electromagnetic fields (PEMFs) in musculoskeletal disorders, Biomed. Pharmacother. 131 (Nov. 2020) 110767, https://doi.org/10.1016/J.BIOPHA.2020.110767.

[5] R. Andrade, et al., Pulsed electromagnetic field therapy effectiveness in low back pain: a systematic review of randomized controlled trials, Porto Biomed. J. 1 (5) (Nov. 2016) 156, https://doi.org/10.1016/J.PBJ.2016.09.001.

[6] B. Strauch, C. Herman, R. Dabb, L.J. Ignarro, A.A. Pilla, Evidence-based use of pulsed electromagnetic field therapy in clinical plastic surgery, Aesthet. Surg. J. 29 (2) (Mar. 2009) 135–143, https://doi.org/10.1016/J.ASJ.2009.02.001/2/10.1016_J.ASJ.2009.02.001-FIG 9.JPEG.

[7] E.R. Larsen, et al., Transcranial pulsed electromagnetic fields for treatment-resistant depression: a multicenter 8-week single-arm cohort study: the eighth trial of the Danish university antidepressant group, Eur. Psychiatry 63 (1) (2020), https://doi.org/10.1192/J.EURPSY.2020.3.

[8] M. Vadalà, J.C. Morales-Medina, A. Vallelunga, B. Palmieri, C. Laurino, T. Iannitti, Mechanisms and therapeutic effectiveness of pulsed electromagnetic field therapy in oncology, Cancer Med. 5 (11) (Nov. 2016) 3128, https://doi.org/10.1002/CAM4.861.

[9] P. Kazimierczak, A. Przekora, Bioengineered living bone grafts—a concise review on bioreactors and production techniques in vitro, Int. J. Mol. Sci. 23 (3) (Feb. 2022), https://doi.org/10.3390/IJMS23031765.

[10] C. Galli, G. Pedrazzi, M. Mattioli-Belmonte, S. Guizzardi, The use of pulsed electromagnetic fields to promote bone responses to biomaterials in vitro and in

vivo, Int. J. Biomater. (2018) 2018, https://doi.org/10.1155/2018/8935750 (Hindawi Limited).

[11] K. Varani, et al., Pulsed Electromagnetic Field Stimulation in Osteogenesis and Chondrogenesis: Signaling Pathways and Therapeutic Implications, 2021, https://doi.org/10.3390/ijms22020809.

[12] L. Caliogna, et al., Pulsed electromagnetic fields in bone healing: Molecular pathways and clinical applications, Int. J. Mol. Sci. 22 (14) (Jul. 02, 2021), https://doi.org/10.3390/ijms22147403 (MDPI).

[13] R. Cadossi, L. Massari, J. Racine-Avila, R.K. Aaron, Pulsed electromagnetic field stimulation of bone healing and joint preservation: cellular mechanisms of skeletal response, J. Am. Acad. Orthop. Surg. Glob. Res. Rev. 4 (5) (2020), https://doi.org/10.5435/JAAOSGlobal-D-19-00155 (Wolters Kluwer Health).

[14] S. Ehnert, et al., Translational insights into extremely low frequency pulsed electromagnetic fields (ELF-PEMFs) for bone regeneration after trauma and orthopedic surgery, J. Clin. Med. 8 (12) (Dec. 2019), https://doi.org/10.3390/JCM8122028.

[15] L. Peng, et al., Effectiveness of pulsed electromagnetic fields on bone healing: a systematic review and meta-analysis of randomized controlled trials, Bioelectromagnetics 41 (5) (Jul. 2020) 323–337, https://doi.org/10.1002/BEM.22271.

[16] W.H. Bailey, Health effects relevant to the setting of EMF exposure limits, Health Phys. 83 (3) (2002) 376–386, https://doi.org/10.1097/00004032-200209000-00007.

[17] D.J. Panagopoulos, Comparing DNA damage induced by mobile telephony and other types of man-made electromagnetic fields, Mutat. Res. Rev. Mutat. Res. 781 (Jul. 2019) 53–62, https://doi.org/10.1016/J.MRREV.2019.03.003.

[18] S. Gabetti, et al., An automated 3D-printed perfusion bioreactor combinable with pulsed electromagnetic field stimulators for bone tissue investigations, Sci. Rep. 12 (1) (Aug. 2022) 1–14, https://doi.org/10.1038/s41598-022-18075-1 (2022 12:1).

[19] R. Pecci, S. Baiguera, P. Ioppolo, R. Bedini, C. Del Gaudio, 3D printed scaffolds with random microarchitecture for bone tissue engineering applications: manufacturing and characterization, J. Mech. Behav. Biomed. Mater. 103 (Mar. 2020) 103583, https://doi.org/10.1016/J.JMBBM.2019.103583.

[20] M. Ledda, et al., Biological response to bioinspired microporous 3D-printed scaffolds for bone tissue engineering, Int. J. Mol. Sci. 23 (10) (May 2022) 5383, https://doi.org/10.3390/IJMS23105383 (2022, Vol. 23, Page 5383).

[21] S. Gabetti, B. Masante, A. Schiavi, E. Scatena, E. Zenobi, S. Israel, A. Sanginario, C. Del Gaudio, A. Audenino, U. Morbiducci, D. Massai, Adaptable test bench for ASTM-compliant permeability measurement of porous scaffolds for tissue engineering, Sci. Rep. 14 (1) (2024) 1722, https://doi.org/10.1038/s41598-024-52159-4.

[22] G.N. Bancroft, V.I. Sikavitsas, J. van den Dolder, T.L. Sheffield, C.G. Ambrose, J. A. Jansen, A.G. Mikos, Fluid flow increases mineralized matrix deposition in 3D perfusion culture of marrow stromal osteoblasts in a dose-dependent manner, Proc. Natl. Acad. Sci. U. S. A. 99 (20) (2002) 12600–12605, https://doi.org/10.1073/pnas.202296599.

[23] C. Wittkowske, G.C. Reilly, D. Lacroix, C.M. Perrault, *In vitro* bone cell models: impact of fluid shear stress on bone formation, Front. Bioeng. Biotechnol. 15 (4) (Nov 2016) 87, https://doi.org/10.3389/fbioe.2016.00087 (PMID: 27896266; PMCID: PMC5108781).

[24] S. James, et al., Multiparameter analysis of human bone marrow stromal cells identifies distinct immunomodulatory and differentiation-competent subtypes, Stem Cell Rep. 4 (6) (Jun. 2015) 1004–1015, https://doi.org/10.1016/J.STEMCR.2015.05.005.

[25] K.J. Livak, T.D. Schmittgen, Analysis of relative gene expression data using real-time quantitative PCR and the $2-\Delta\Delta CT$ method, Methods 25 (4) (Dec. 2001) 402–408, https://doi.org/10.1006/METH.2001.1262.

[26] T. Schmittgen, K. Livak, Analyzing real-time PCR data by comparative CT method, Nat. Protoc. 3 (Jun. 2008) 1101–1108.

[27] S. Andrews, FASTQC: a quality control tool for high throughput sequence data, Available online at, http://www.bioinformatics.babraham.ac.uk/projects/fastqc/.

[28] P. Ewels, M. Magnusson, S. Lundin, M. Käller, MultiQC: summarize analysis results for multiple tools and samples in a single report, Bioinformatics 32 (19) (Oct. 2016) 3047, https://doi.org/10.1093/BIOINFORMATICS/BTW354.

[29] B. Li, C.N. Dewey, RSEM: accurate transcript quantification from RNA-Seq data with or without a reference genome, BMC Bioinformatics 12 (1) (Aug. 2011) 1–16, https://doi.org/10.1186/1471-2105-12-323/TABLES/6.

[30] F. Cunningham, et al., Ensembl 2022, Nucleic Acids Res. 50 (D1) (Jan. 2022) D988, https://doi.org/10.1093/NAR/GKAB1049.

[31] A. Dobin, et al., STAR: ultrafast universal RNA-seq aligner, Bioinformatics 29 (1) (Jan. 2013) 15–21, https://doi.org/10.1093/BIOINFORMATICS/BTS635.

[32] M.I. Love, W. Huber, S. Anders, Moderated estimation of fold change and dispersion for RNA-seq data with DESeq2, Genome Biol. 15 (12) (Dec. 2014) 550, https://doi.org/10.1186/S13059-014-0550-8.

[33] Y. Zhou, et al., Metascape provides a biologist-oriented resource for the analysis of systems-level datasets, Nat. Commun. 10 (1) (Apr. 2019) 1–10, https://doi.org/10.1038/s41467-019-09234-6 (2019 10:1).

[34] J. Chen, E.E. Bardes, B.J. Aronow, A.G. Jegga, ToppGene suite for gene list enrichment analysis and candidate gene prioritization, Nucleic Acids Res. 37 (suppl_2) (Jul. 2009) W305–W311, https://doi.org/10.1093/NAR/GKP427.

[35] F. Supek, M. Bošnjak, N. Škunca, T. Šmuc, REVIGO summarizes and visualizes long lists of gene ontology terms, PloS One 6 (7) (2011) e21800, https://doi.org/10.1371/JOURNAL.PONE.0021800.

[36] C.S. Bahney, et al., Cellular biology of fracture healing, J. Orthop. Res. 37 (1) (Jan. 2019) 35, https://doi.org/10.1002/JOR.24170.

[37] M. De Mattei, et al., Pulsed electromagnetic fields modulate miRNAs during osteogenic differentiation of bone mesenchymal stem cells: a possible role in the osteogenic-angiogenic coupling, Stem Cell Rev. Rep. 16 (5) (Oct. 2020) 1005–1012, https://doi.org/10.1007/S12015-020-10009-6/FIGURES/3.

[38] A. Marintchev, T. Ito, eIF2B and the integrated stress response: a structural and mechanistic view, Biochemistry 59 (13) (Apr. 2020) 1299, https://doi.org/10.1021/ACS.BIOCHEM.0C00132.

[39] M.J. Vinolo-Gil, M. Rodríguez-Huguet, C. García-Muñoz, G. Gonzalez-Medina, F. J. Martin-Vega, R. Martín-Valero, Effects of peripheral electromagnetic fields on spasticity: a systematic review, J. Clin. Med. 11 (13) (Jun. 2022) 3739, https://doi.org/10.3390/JCM11133739 (2022, Vol. 11, Page 3739).

[40] M. Cámara-Torres, R. Sinha, C. Mota, L. Moroni, Improving cell distribution on 3D additive manufactured scaffolds through engineered seeding media density and viscosity, Acta Biomater. 101 (Jan. 2020) 183–195, https://doi.org/10.1016/J.ACTBIO.2019.11.020.

[41] F. Fahimipour, et al., Enhancing cell seeding and osteogenesis of MSCs on 3D printed scaffolds through injectable BMP2 immobilized ECM-mimetic gel, Dent. Mater. 35 (7) (Jul. 2019) 990–1006, https://doi.org/10.1016/J.DENTAL.2019.04.004.

[42] M.K. Hsieh, et al., Bone regeneration in ds-red pig calvarial defect using allogenic transplantation of EGFP-pMSCs – a comparison of host cells and seeding cells in the scaffold, PloS One 14 (7) (Jul. 2019), https://doi.org/10.1371/JOURNAL.PONE.0215499.

[43] H. Wu, et al., The dose–effect relationship between the seeding quantity of human marrow mesenchymal stem cells and in vivo tissue-engineered bone yield, Cell Transplant. 24 (10) (Oct. 2015) 1957–1968, https://doi.org/10.3727/096368914X685393/ASSET/IMAGES/LARGE/10.3727_096368914X685393-FIG2.JPEG.

[44] K.T. Lim, D.K. Patel, H. Seonwoo, J. Kim, J.H. Chung, A fully automated bioreactor system for precise control of stem cell proliferation and differentiation, Biochem. Eng. J. 150 (Oct. 2019) 107258, https://doi.org/10.1016/J.BEJ.2019.107258.

[45] J.R. Vetsch, D.C. Betts, R. Müller, S. Hofmann, Flow velocity-driven differentiation of human mesenchymal stromal cells in silk fibroin scaffolds: a combined experimental and computational approach, PloS One 12 (7) (Jul. 2017), https://doi.org/10.1371/JOURNAL.PONE.0180781.

[46] L. Bjerre, C.E. Bünger, M. Kassem, T. Mygind, Flow perfusion culture of human mesenchymal stem cells on silicate-substituted tricalcium phosphate scaffolds, Biomaterials 29 (17) (Jun. 2008) 2616–2627, https://doi.org/10.1016/J.BIOMATERIALS.2008.03.003.

[47] F. Zhao, B. van Rietbergen, K. Ito, S. Hofmann, Flow rates in perfusion bioreactors to maximise mineralisation in bone tissue engineering in vitro, J. Biomech. 79 (Oct. 2018) 232–237, https://doi.org/10.1016/J.JBIOMECH.2018.08.004.

[48] A. Ongaro, A. Pellati, L. Bagheri, C. Fortini, S. Setti, M. De Mattei, Pulsed electromagnetic fields stimulate osteogenic differentiation in human bone marrow and adipose tissue derived mesenchymal stem cells, Bioelectromagnetics 35 (6) (Sep. 2014) 426–436, https://doi.org/10.1002/BEM.21862.

[49] K.S. Kang, J.M. Hong, J.A. Kang, J.W. Rhie, Y.H. Jeong, D.W. Cho, Regulation of osteogenic differentiation of human adipose-derived stem cells by controlling electromagnetic field conditions, Exp. Mol. Med. 45 (1) (2013) e6, https://doi.org/10.1038/EMM.2013.11.

[50] J.H.W. Jansen, et al., Stimulation of osteogenic differentiation in human osteoprogenitor cells by pulsed electromagnetic fields: an in vitro study, BMC Musculoskelet. Disord. 11 (1) (Aug. 2010) 1–11, https://doi.org/10.1186/1471-2474-11-188/FIGURES/6.

[51] L.Y. Sun, D.K. Hsieh, P.C. Lin, H.T. Chiu, T.W. Chiou, Pulsed electromagnetic fields accelerate proliferation and osteogenic gene expression in human bone marrow mesenchymal stem cells during osteogenic differentiation, Bioelectromagnetics 31 (3) (Apr. 2010) 209–219, https://doi.org/10.1002/BEM.20550.

[52] M.T. Tsai, W.J. Li, R.S. Tuan, W.H. Chang, Modulation of osteogenesis in human mesenchymal stem cells by specific pulsed electromagnetic field stimulation, J. Orthop. Res. 27 (9) (Sep. 2009) 1169–1174, https://doi.org/10.1002/JOR.20862.

[53] E. Kaivosoja, V. Sariola, Y. Chen, Y.T. Konttinen, The effect of pulsed electromagnetic fields and dehydroepiandrosterone on viability and osteo-induction of human mesenchymal stem cells, J. Tissue Eng. Regen. Med. 9 (1) (Jan. 2015) 31–40, https://doi.org/10.1002/TERM.1612.

[54] J. Yan, L. Dong, B. Zhang, N. Qi, "Effects of Extremely Low-Frequency Magnetic Field on Growth and Differentiation of Human Mesenchymal Stem Cells," https://doi.org/10.3109/01676830.2010.505490 29, Dec. 2010, pp. 165–176, https://doi.org/10.3109/01676830.2010.505490 (no. 4).

[55] Z. Schwartz, M. Fisher, C.H. Lohmann, B.J. Simon, B.D. Boyan, Osteoprotegerin (OPG) production by cells in the osteoblast lineage is regulated by pulsed electromagnetic fields in cultures grown on calcium phosphate substrates, Ann. Biomed. Eng. 37 (3) (Mar. 2009) 437–444, https://doi.org/10.1007/S10439-008-9628-3/FIGURES/5.

[56] S. Ehnert, et al., Translational insights into extremely low frequency pulsed electromagnetic fields (ELF-PEMFs) for bone regeneration after trauma and orthopedic surgery, J. Clin. Med. 8 (12) (Nov. 2019) 2028, https://doi.org/10.3390/JCM8122028 (2019, Vol. 8, Page 2028).

[57] N. Bloise, et al., The effect of pulsed electromagnetic field exposure on osteoinduction of human mesenchymal stem cells cultured on nano-TiO2 surfaces, PloS One 13 (6) (Jul. 2018), https://doi.org/10.1371/JOURNAL.PONE.0199046.

[58] Z. Schwartz, B.J. Simon, M.A. Duran, G. Barabino, R. Chaudhri, B.D. Boyan, Pulsed electromagnetic fields enhance BMP-2 dependent osteoblastic differentiation of human mesenchymal stem cells, J. Orthop. Res. 26 (9) (Sep. 2008) 1250–1255, https://doi.org/10.1002/JOR.20591.

[59] M. Arjmand, A. Ardeshirylajimi, H. Maghsoudi, E. Azadian, Osteogenic differentiation potential of mesenchymal stem cells cultured on nanofibrous scaffold improved in the presence of pulsed electromagnetic field, J. Cell. Physiol. 233 (2) (Feb. 2018) 1061–1070, https://doi.org/10.1002/JCP.25962.

[60] H. Wang, et al., Enhanced osteogenesis of bone marrow stem cells cultured on hydroxyapatite/collagen I scaffold in the presence of low-frequency magnetic field, J. Mater. Sci. Mater. Med. 30 (8) (Aug. 2019) 1–12, https://doi.org/10.1007/S10856-019-6289-8/FIGURES/10.

[61] M.T. Tsai, W.H.S. Chang, K. Chang, R.J. Hou, T.W. Wu, Pulsed electromagnetic fields affect osteoblast proliferation and differentiation in bone tissue engineering, Bioelectromagnetics 28 (7) (Oct. 2007) 519–528, https://doi.org/10.1002/BEM.20336.

[62] A. Ongaro, et al., Electromagnetic fields (EMFs) and adenosine receptors modulate prostaglandin E2 and cytokine release in human osteoarthritic synovial fibroblasts, J. Cell. Physiol. 227 (6) (Jun. 2012) 2461–2469, https://doi.org/10.1002/JCP.22981.

[63] K. Varani, et al., Adenosine receptors as a biological pathway for the anti-inflammatory and beneficial effects of low frequency low energy pulsed electromagnetic fields, Mediators Inflamm. 2017 (2017), https://doi.org/10.1155/2017/2740963.

[64] L. Ferroni, et al., Pulsed electromagnetic fields increase osteogenetic commitment of MSCs via the mTOR pathway in TNF-α mediated inflammatory conditions: an in-vitro study, Sci. Rep. 8 (1) (Mar. 2018) 1–13, https://doi.org/10.1038/s41598-018-23499-9 (2018 8:1).

[65] L. Gerdesmeyer, et al., "Stimulation of Human Bone Marrow Mesenchymal Stem Cells by Electromagnetic Transduction Therapy - EMTT," https://doi.org/10.1080/15368378.2022.2079672 41, 2022, pp. 304–314, https://doi.org/10.1080/15368378.2022.2079672 (no. 3).

[66] O.M. Tepper, et al., Electromagnetic fields increase in vitro and in vivo angiogenesis through endothelial release of FGF-2, FASEB J. 18 (11) (Aug. 2004) 1231–1233, https://doi.org/10.1096/FJ.03-0847FJE.

[67] S. Wu, Q. Yu, A. Lai, J. Tian, Pulsed electromagnetic field induces Ca2+−dependent osteoblastogenesis in C3H10T1/2 mesenchymal cells through the Wnt-Ca2+/Wnt-β-catenin signaling pathway, Biochem. Biophys. Res. Commun. 503 (2) (Sep. 2018) 715–721, https://doi.org/10.1016/J.BBRC.2018.06.066.

[68] M. Wu, G. Chen, Y.P. Li, TGF-β and BMP signaling in osteoblast, skeletal development, and bone formation, homeostasis and disease, Bone Res. 4 (1) (Apr. 2016) 1–21, https://doi.org/10.1038/boneres.2016.9 (2016 4:1).

[69] K. Maeda, et al., The regulation of bone metabolism and disorders by Wnt signaling, Int. J. Mol. Sci. 20 (22) (Nov. 2019) 5525, https://doi.org/10.3390/IJMS20225525 (2019, Vol. 20, Page 5525).

[70] E. Jimi, T. Katagiri, Critical roles of NF-κB signaling molecules in bone metabolism revealed by genetic mutations in osteopetrosis, Int. J. Mol. Sci. 23 (14) (Jul. 2022) 7995, https://doi.org/10.3390/IJMS23147995 (2022, Vol. 23, Page 7995).

[71] M.A. Icer, M. Gezmen-Karadag, The multiple functions and mechanisms of osteopontin, Clin. Biochem. 59 (Sep. 2018) 17–24, https://doi.org/10.1016/J.CLINBIOCHEM.2018.07.003.